ELSEVIER

Journal of Alloys and Compounds 438 (2007) 129–141

Journal of ALLOYS AND COMPOUNDS

www.elsevier.com/locate/jallcom

Thermodynamic assessments of the Cu–Mn–X (X: Fe, Co) systems

C.P. Wang [a], X.J. Liu [a,*], I. Ohnuma [b], R. Kainuma [b], K. Ishida [b]

[a] *Department of Materials Science and Engineering, College of Chemistry and Chemical Engineering, Xiamen University, Xiamen 361005, PR China*
[b] *Department of Materials Science, Graduate School of Engineering, Tohoku University, Sendai 980-8579, Japan*

Received 23 May 2006; received in revised form 9 August 2006; accepted 9 August 2006
Available online 26 December 2006

Abstract

The thermodynamic assessments of the Cu–Mn binary, Cu–Mn–Fe and Cu–Mn–Co ternary systems were carried out by using CALPHAD (calculation of phase diagrams) method on the basis of the experimental data including the thermodynamic properties and phase equilibria. The Gibbs free energies of the liquid, bcc, fcc, hcp, (αMn) and (βMn) phases are described by the subregular solution model. The thermodynamic parameters of the Cu–Mn binary, Cu–Mn–Fe and Cu–Mn–Co ternary systems have been optimized for reproducing the experimental results in each system, respectively. An agreement between the calculated results and experimental data is obtained.

Keywords: Phase equilibria; Phase diagram; Metastable miscibility gap; CALPHAD method; Thermodynamic calculation

1. Introduction

The Cu–Mn system is an important basis for the development of the Cu-based high conduction alloys and Mn-based high damping capacity alloys [1–7]. Fe and Co are important alloy elements to improve the properties of the high damping and workability in the Cu–Mn base alloys [3,5–7]. In addition, the Cu–Mn–Co and Cu–Mn–Fe systems are of importance for the development of the Cu–Co and Cu–Fe base magnetic alloys.

The considerable investigations have been contributed to the phase equilibria in the Cu–Mn system [8–12]. A summary on the phase equilibria and thermodynamic properties of this system was made by Gokcen [13], as shown in Fig. 1. Although the investigations on the thermodynamic properties and phase equilibria in the Cu–Mn system as well as the Cu–Mn–Fe and Cu–Mn–Co systems have been reported, the thermodynamic assessment on these systems are inadequate.

The CALPHAD (calculation of phase diagrams) method is an important tool in the design and evaluation of various materials because it significantly decreases the amount of required experimental work [14]. Recently, the present authors have developed a thermodynamic database of the Cu-based alloys including Cu–Fe–X, Cu–Cr–X, Cu–Ni–X and Cu–Co–X systems within the framework of the CALPHAD method [15–21], which is important for the design and development of Cu-based alloys. As a part of development of the thermodynamic database of Cu-based alloys, the purpose of the present work is to present the thermodynamic assessment of the Cu–Mn binary system as well as the Cu–Mn–Fe and Cu–Mn–Co ternary systems based on the available experimental data.

2. Previous thermodynamic assessments of Cu–Mn–X (X: Fe, Co) system

2.1. The Cu–Mn system

Three previous works on the thermodynamic calculation of this system in the light of CALPHAD method were performed [22–25]. The earlier pioneer work was conducted by Kaufman [22], who produced a satisfactory agreement between the calculated and experimental data on phase equilibria. However, the thermodynamic data for pure Cu and Mn used in Ref. [22] have subsequently been revised by Dinsdale [26]. The other two calculations of this system were made by Lewin et al. [23] and Vřešťál [24], respectively. However, these assessments were mainly used to discuss the measured thermodynamic data, the calculated details were not given. Miettinen [25] reassessed the phase diagram in the Cu–Mn system, however, the calculated results are not in agreement with the Cu–Mn binary system

* Corresponding author.
E-mail address: lxj@xmu.edu.cn (X.J. Liu).

0925-8388/$ – see front matter © 2006 Published by Elsevier B.V.
doi:10.1016/j.jallcom.2006.08.018

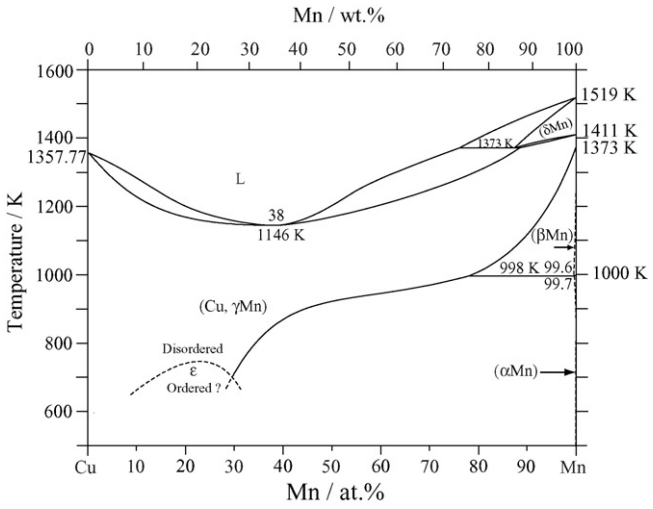

Fig. 1. Cu–Mn binary phase diagram reviewed by Gokcen [13].

reviewed by Gokcen [13]. Other thermodynamic calculations [27,28] concerning the liquid/fcc phase equilibria were also performed, but the calculated results of phase equilibria at low temperature were not given.

2.2. The Cu–Mn–X (X: Fe, Co) system

The thermodynamic assessments of the Cu–Mn–Fe system were made by some investigators [27–29]. However, the lattice stability parameters in the calculation of Hasebe and Nishsawa [27] differ from the lattice stability parameters adopted for Cu, Mn, and Fe in the Scientific Group Thermodata Europe (SGTE) database [26]. In the assessment of Ohtani et al. [28], the calculation can be carried out above 1273 K because the assessment of the Cu–Mn system was only carried out for the liquid, bcc and fcc phases above 1273 K. In addition, in the Ohtani's work the stable miscibility gap of the liquid phase appears in the calculated isothermal section at 1573 K, however, the experimental results indicate that there exists no stable miscibility gap in this system [18,30]. Miettinen [29] made a thermodynamic description in the Cu–Fe side, however, the thermodynamic assessment of the phase equilibria in the Mn-rich part was not carried out, and some available experimental data were ignored in his calculation.

The lattice stability parameters in the thermodynamic assessment of the Cu–Mn–Co system by Hasebe et al. [31] also differ from those reviewed by Dinsdale [26].

3. Evaluation and selection of experimental information

3.1. The Cu–Mn system

Two detailed investigations on the phase equilibria in this system were performed by Grube et al. [8] and Dean et al. [9], respectively. The Cu–Mn phase diagram was reviewed by Gokcen [13] based mainly on these works. The present assessment is mainly based on these experimental data of the phase equilibria.

Some investigations on thermodynamic properties of the liquid and fcc phases were carried out [32–36]. Spencer and Pratt [33] found that the activities of Mn show the strong positive deviation from ideality in the Mn-rich part, but show the negative deviation in the Cu-rich alloys. Such a characteristic feature of activity was explained by the transformation from ferromagnetic to antiferromagnetic states. However, Spencer and Pratt [33] also pointed out that the true activities in the Mn-rich portion maybe slightly lower than observed ones. The activities of Mn measured by Okajima and Sakao [35] almost agree ones by Spencer and Pratt [33] in the most composition ranges. Peters and Wiles [37] studied the vapor pressure of Mn in the fcc phase at high temperature, and found that the activities between 20 and 30 at.% Mn (17.8–27.0 wt.% Mn) sharply increase, which shows the same tendency with that in the liquid phase. Kremzer and Jool [34] and Hajra [36] determined the activities of Mn and Cu at different temperature ranges, respectively, which shows a basic agreement with each other. The experimental data reported in Refs. [33–36] were used in the present assessment with different weights. Scheil and Normann [32] measured the heat capacity of the fcc phase containing 23.1 at.% Mn (20.6 wt.% Mn) at 293–823 K, and observed a λ-shape at 523 K, which was explained due to short-range ordering. These data were used in the present assessment except the data on the ordering. Vitek and Warlimont [5] determined the presence of a metastable miscibility gap of the fcc phase in two-phase region (αMn + fcc) on the basis of TEM observation and hardness measurement. However, no further works confirm this conclusion, and Vitek's work was not included in the review by Gokcen [13]. Therefore, the data were not used in this assessment.

3.2. The Cu–Mn–X (X: Fe, Co) system

3.2.1. Cu–Mn–Fe system

Salter [38] measured the solid/liquid distribution equilibrium of the Cu–Mn–Fe ternary system by using mild steels. Hasebe and Nishizawa [27] investigated the isothermal section diagrams at 1173–1323 K by the diffusion couple method. How-

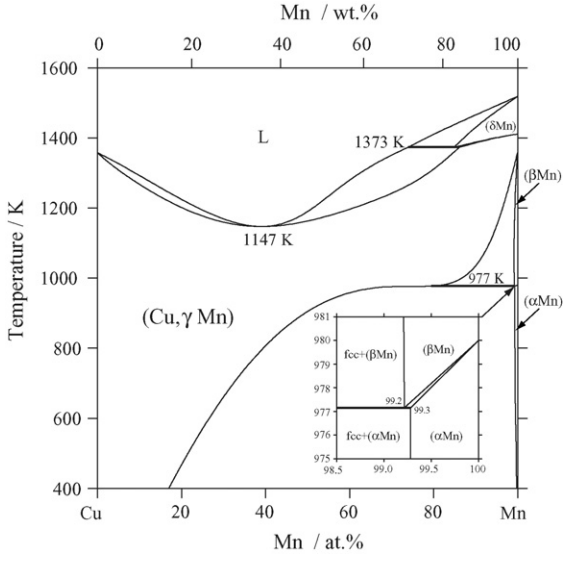

Fig. 2. Calculated stable phase diagram of the Cu–Mn system by the present assessment.

Table 1
Thermodynamic parameters in the Cu–Mn–X (Fe, Co) ternary system

	Reference
Liquid phase: $(Cu, Fe, Mn)_1$ and $(Co, Cu, Mn)_1$	
$L^{L}_{Cu,Mn} = (-25300 + 18.5T) + (-16300 + 5T)(x_{Cu} - x_{Mn}) + (-1620.565 - 0.57T)(x_{Cu} - x_{Mn})^2$	This work
$L^{L}_{Cu,Fe} = (+35625.8 - 2.19045T) + (-1529.8 + 1.15291T)(x_{Cu} - x_{Fe}) + (+12714.4 - 5.18624T)(x_{Cu} - x_{Fe})^2 + (+1177.1)(x_{Cu} - x_{Fe})^3$	[53]
$L^{L}_{Co,Cu} = (+35200 - 4.945T) + (-1000 + 0.083T)(x_{Co} - x_{Cu})$	[58]
$L^{L}_{Fe,Mn} = (-3950 + 0.489T) + (+1145)(x_{Fe} - x_{Mn})$	[61]
$L^{L}_{Co,Mn} = -29476$	[65]
$L^{L}_{Cu,Fe,Mn} = (+241298 - 140T)x_{Cu} + (+82096 - 40T)x_{Fe} + (+25901.5 - 20T)x_{Mn}$	This work
$L^{L}_{Co,Cu,Mn} = (-14000)x_{Co} + (+41625 - 42.5T)x_{Cu} + (-29000)x_{Mn}$	This work
Fcc phase (A1): $(Cu, Fe, Mn)_1$ and $(Co, Cu, Mn)_1$	
$L^{fcc}_{Cu,Mn} = (+8642.66 - 2T) + (-13000 + 3.1042T)(x_{Cu} - x_{Mn})$	This work
$T^{fcc}_{c} = -1620x_{Mn}$	
$\beta^{fcc} = -1.86x_{Mn}$	
$L^{fcc}_{Cu,Fe} = (+43319.6 - 6.94445T) + (+6068.8 + 2.83662T)(x_{Cu} - x_{Fe}) + (+3629.4)(x_{Cu} - x_{Fe})^2$	[53]
$T^{fcc}_{c} = -201x_{Fe}$	
$\beta^{fcc} = -2.1x_{Fe}$	
$L^{fcc}_{Co,Cu} = (+40900 - 5.5T) + (-1600)(x_{Co} - x_{Cu}) + (-6900)(x_{Co} - x_{Cu})^2$	[58]
$T^{fcc}_{c} = +1396x_{Co}$	
$\beta^{fcc} = +1.35x_{Co}$	
$L^{fcc}_{Fe,Mn} = (-7762 + 3.865T) + (-259)(x_{Fe} - x_{Mn})$	[61]
$T^{fcc}_{c} = (-201)x_{Fe} + (-1620)x_{Mn} + [(-2282) + (-2068)(x_{Fe} - x_{Mn})]x_{Fe}x_{Mn}$	
$\beta^{fcc} = (-2.1)x_{Fe} + (-1.86)x_{Mn}$	
$L^{fcc}_{Co,Mn} = (-23756) + (-2343)(x_{Co} - x_{Mn})$	[65]
$T^{fcc}_{c} = (+1396)x_{Co} + (-1620)x_{Mn} + [(-2685) + 3657(x_{Co} - x_{Mn})]x_{Co}x_{Mn}$	
$\beta^{fcc} = (+1.35)x_{Co} + (-1.86)x_{Mn} + (-1.07)x_{Co}x_{Mn}$	
$L^{fcc}_{Cu,Fe,Mn} = (-60000 + 105T)x_{Cu} + (-121140 + 89T)x_{Fe} + (-160467 + 112T)x_{Mn}$	This work
$L^{fcc}_{Co,Cu,Mn} = (-86000 + 40T)x_{Co} + (-157000 + 100T)x_{Cu} + (-224500 + 150T)x_{Mn}$	This work
Bcc phase (A2): $(Cu, Fe, Mn)_1$ and $(Co, Cu, Mn)_1$	
$L^{bcc}_{Cu,Mn} = (+5465.442 - 3.254T) + (-20992 + 7T)(x_{Cu} - x_{Mn})$	This work
$T^{bcc}_{c} = -580x_{Mn}$	
$\beta^{bcc} = -0.27x_{Mn}$	
$L^{bcc}_{CuFe} = +39676 - 4.73222T$	[53]
$T^{bcc}_{c} = (+1043)x_{Fe} + (-41.4)x_{Cu}x_{Fe}$	
$\beta^{bcc} = +2.22x_{Fe}$	
$L^{bcc}_{Co,Cu} = +35000$	This work
$T^{bcc}_{c} = +1450x_{Co}$	
$\beta^{bcc} = +1.35x_{Co}$	
$L^{bcc}_{Fe,Mn} = -2759 + 1.237T$	[61]
$T^{bcc}_{c} = (+1043)x_{Fe} + (-580)x_{Mn} + (+123)x_{Fe}x_{Mn}$	
$\beta^{bcc} = (+2.22)x_{Fe} + (-0.27)x_{Mn}$	
$L^{bcc}_{Co,Mn} = -23945$	[65]
$T^{bcc}_{c} = (+1450)x_{Co} + (-580)x_{Mn}$	
$\beta^{bcc} = (+1.35)x_{Co} + (-0.27)x_{Mn}$	
$L^{bcc}_{Cu,Fe,Mn} = (+20000 + 1.15T)x_{Cu} + (+20000 + 1.15T)x_{Fe} + (+20000 + 1.15T)x_{Mn}$	This work
$L^{bcc}_{Co,Cu,Mn} = (+5000)x_{Co} + (+5000)x_{Cu} + (+5000)x_{Mn}$	This work
Hcp phase (A3): $(Cu, Fe, Mn)_1$ and $(Co, Cu, Mn)_1$	
$L^{hcp}_{Cu,Mn} = +13000$	This work
$T^{hcp}_{c} = -1620x_{Mn}$	
$\beta^{hcp} = -1.86x_{Mn}$	
$L^{hcp}_{CuFe} = +40000 - 4T$	This work
$L^{hcp}_{Co,Cu} = +28000$	This work
$T^{hcp}_{c} = +1396x_{Co}$	
$\beta^{hcp} = +1.35x_{Co}$	

Table 1 (*Continued*)

	Reference
$L^{hcp}_{Fe,Mn} = (-5582 + 3.865T) + (+273)(x_{Fe} - x_{Mn})$	[61]
$T_c^{hcp} = -1620x_{Mn}$	
$\beta^{hcp} = -1.86x_{Mn}$	
$L^{hcp}_{Co,Mn} = (-21000) + (-4000)(x_{Co} - x_{Mn})$	[65]
$T_c^{bcc} = (+1396)x_{Co} + (-1620)x_{Mn} + [(-2685) + (+3657)(x_{Co} - x_{Mn})]x_{Co}x_{Mn}$	
$\beta^{bcc} = (+1.35)x_{Co} + (-1.86)x_{Mn} + (-1.07)x_{Co}x_{Mn}$	
$L^{hcp}_{Cu,Fe,Mn} = 0$	This work
$L^{hcp}_{Co,Cu,Mn} = (+5000)x_{Co} + (+5000)x_{Cu} + (+5000)x_{Mn}$	This work
βMn phase (A13): (Cu, Fe, Mn)$_1$ and (Co, Cu, Mn)$_1$	
$L^{\beta Mn}_{Cu,Mn} = (+53000 - 10T) + (+13519.89)(x_{Cu} - x_{Mn})$	This work
$L^{\beta Mn}_{CuFe} = +80000 + 20T$	This work
$L^{\beta Mn}_{Co,Cu} = +30000$	This work
$L^{\beta Mn}_{Fe,Mn} = -11518 + 2.819T$	[61]
$L^{\beta Mn}_{Co,Mn} = (-26772 - 2.39T) + (-3243)(x_{Co} - x_{Mn})$	[65]
$L^{\beta Mn}_{Cu,Fe,Mn} = 0$	This work
$L^{\beta Mn}_{Co,Cu,Mn} = (-3000)x_{Co} + (-3000)x_{Cu} + (-5000)x_{Mn}$	This work
αMn phase (A12): (Cu, Fe, Mn)$_1$ and (Co, Cu, Mn)$_1$	
$L^{\alpha Mn}_{Cu,Mn} = -1000 + 26T$	This work
$T_c^{\alpha Mn} = -285x_{Mn}$	
$\beta^{\alpha Mn} = -0.66x_{Mn}$	
$L^{\alpha Mn}_{CuFe} = +60000$	This work
$L^{\alpha Mn}_{Co,Cu} = +5000$	This work
$L^{\alpha Mn}_{Fe,Mn} = -10184$	[61]
$T_c^{\alpha Mn} = -285x_{Mn}$	
$\beta^{\alpha Mn} = -0.66x_{Mn}$	
$L^{\alpha Mn}_{Co,Mn} = -18335$	[65]
$T_c^{\alpha Mn} = -285x_{Mn}$	
$\beta^{\alpha Mn} = -0.66x_{Mn}$	
$L^{\alpha Mn}_{Cu,Fe,Mn} = 0$	This work
$L^{\alpha Mn}_{Co,Cu,Mn} = 0$	This work

Note: All parameter values are given in SI units (J mol^{-1}). Parameters for pure elements are taken from Ref. [26].

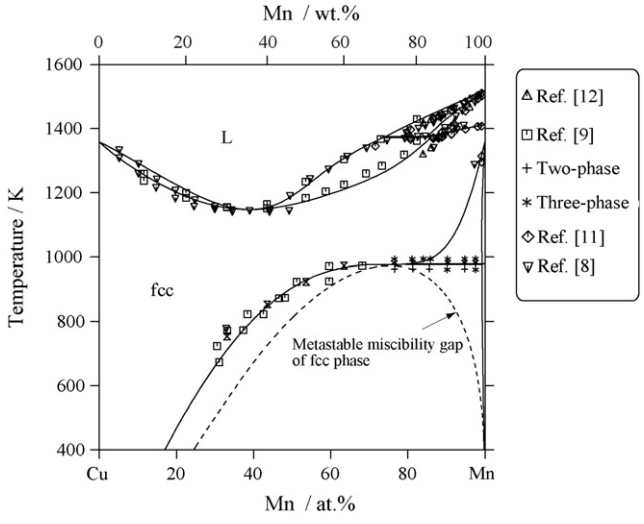

Fig. 3. Calculated Cu–Mn phase diagram with a metastable miscibility gap of fcc phase with the experimental data.

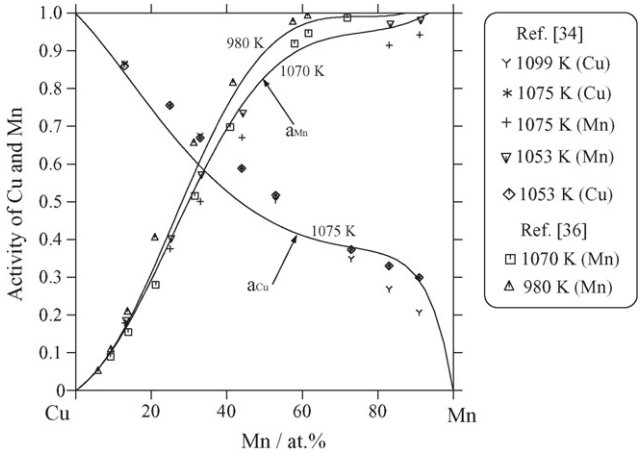

Fig. 4. Calculated Cu and Mn activities in the fcc phase compared with the experimental data. The reference states for copper and manganese are pure fcc Cu and pure (βMn), respectively.

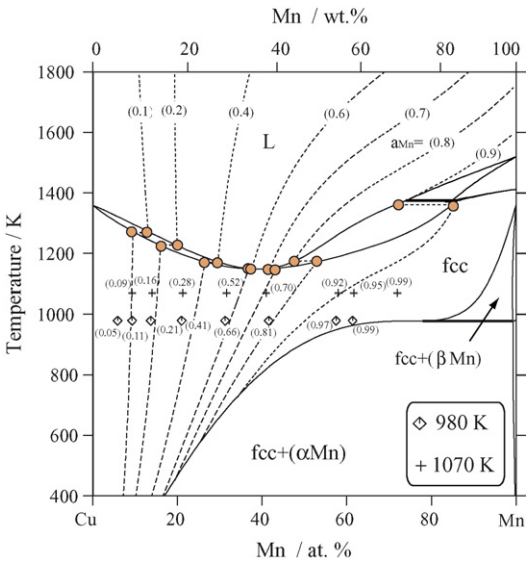

Fig. 5. Calculated iso-activities of Mn in fcc and liquid phases compared with the experimental data [36]. The reference state is pure (βMn).

ever, the extrapolation of those experimental data to the Cu–Mn binary side does not agree so well with the binary data. Recently Ohtani et al. [28] investigated the liquid/solid phase equilibrium at 1373, 1473, and 1573 K by the diffusion couple method. Wang [18] also determined the phase equilibria in the Cu–Fe side by metallurgical method. Parravano [39] determined some vertical sections using thermal analysis. No ternary phases and thermodynamic properties were reported in this system. On the basis of these experimental data, the phase equilibria in the Cu–Mn–Fe ternary system were reviewed in Refs. [40–43]. The experimental data reported in Refs. [18,27,28,38,39,41,43] were used in the present assessment.

3.2.2. Cu–Mn–Co system

Hasebe et al. [31] and Oikawa [44] investigated the isothermal section diagrams in the Cu–Mn–Co system at 1150–1550 K by the diffusion couple technique and metallurgical methods. However, as the same with the Cu–Mn–Fe system, the extrapolation of those experimental data to the Cu–Mn binary side also does not agree well with the binary data. Köster and Wagner [45] investigated the phase equilibria in the composition range of 10–40 wt.% Mn by means of thermal, magnetic and microstructural analyses, and gave four vertical sections at 10, 20, 30 and 40 wt.% Mn. No ternary phases and thermodynamic properties of the Cu–Mn–Co system were reported. These studies for the Cu–Mn–Co ternary system were respectively reviewed in Refs. [46,47]. The data of the phase equilibria reported in references [31,44–46] were used in the present calculation.

4. Thermodynamic modeling

The Gibbs free energies of the liquid, bcc, fcc, hcp, (αMn) and (βMn) phases in the ternary Cu–Mn–X system are described by the subregular solution model with the Redlich–Kister formula [48], as follows:

$$G_m^{\phi} = \sum_{i=\mathrm{Cu,Mn,X}} {}^0G_i^{\phi} x_i + RT \sum_{i=\mathrm{Cu,Mn,X}} x_i \ln x_i + L^{\phi}_{\mathrm{CuMn}} x_{\mathrm{Cu}} x_{\mathrm{Mn}} + L^{\phi}_{\mathrm{CuX}} x_{\mathrm{Cu}} x_{\mathrm{X}} + L^{\phi}_{\mathrm{MnX}} x_{\mathrm{Mn}} x_{\mathrm{X}} + L^{\phi}_{\mathrm{CuMnX}} x_{\mathrm{Cu}} x_{\mathrm{Mn}} x_{\mathrm{X}} + \Delta^{\mathrm{mag}} G \quad (1)$$

where ${}^0G_i^{\phi}$ is the Gibbs free energy of pure component i in the respective reference state with the ϕ phase. The Gibbs free energy of pure component i in its different phase states is taken from the SGTE database [26]. R is the gas constant, and T is the absolute temperature. x_i is the mole fraction of component i, and L_{ij}^{ϕ} and $L^{\phi}_{\mathrm{CuMnX}}$ are the temperature and composition dependent interaction energy in binary and ternary systems, respectively. The temperature and composition dependence of the parameters

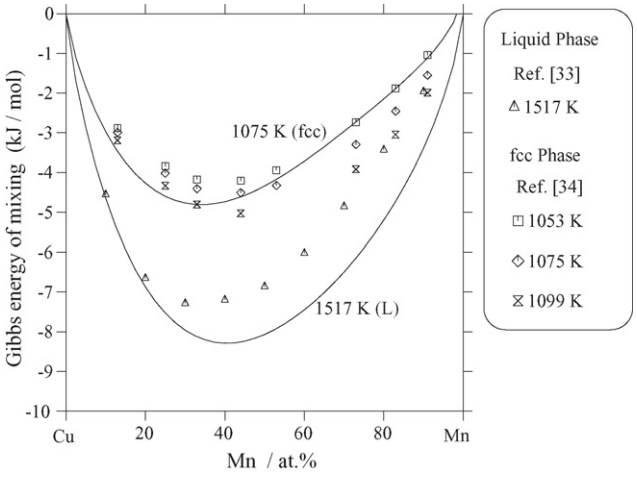

Fig. 6. Calculated Gibbs free energies of mixing of fcc (reference states: pure fcc Cu for copper and pure (βMn) for manganese) and liquid phases (reference state: liquid phase for pure Cu and Mn) compared with the experimental data.

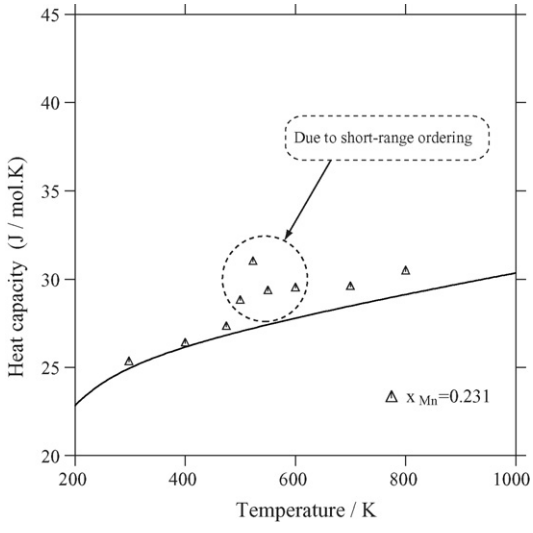

Fig. 7. Calculated heat capacity of fcc phase vs. temperature compared with the experimental data [32].

L_{ij}^{ϕ} and $L_{\mathrm{CuMnX}}^{\phi}$ are expressed in the following forms:

$$L_{ij}^{\phi} = {}^{0}L_{ij}^{\phi} + {}^{1}L_{ij}^{\phi}(x_i^{\phi} - x_j^{\phi}) + {}^{2}L_{ij}^{\phi}(x_i^{\phi} - x_j^{\phi})^2 + \cdots = \sum_{m=0}^{n} {}^{m}L_{ij}^{\phi}(x_i^{\phi} - x_j^{\phi})^m \quad (2)$$

$${}^{m}L_{ij}^{\phi} = a + bT + cT\ \ln\ T \quad (3)$$

$$L_{\mathrm{CuMnX}}^{\phi} = {}^{0}L_{\mathrm{CuMnX}}^{\phi}x_{\mathrm{Cu}} + {}^{1}L_{\mathrm{CuMnX}}^{\phi}x_{\mathrm{Mn}} + {}^{2}L_{\mathrm{CuMnX}}^{\phi}x_{\mathrm{X}} \quad (4)$$

$${}^{n}L_{\mathrm{CuMnX}}^{\phi} = a' + b'T \quad (5)$$

$\Delta^{\mathrm{mag}}G$ is the magnetic contribution to the Gibbs free energy, which is described by the following equation [49]:

$$\Delta^{\mathrm{mag}}G = RT\ \ln(\beta + 1)f(\tau) \quad (6)$$

where the function $f(\tau)$ is formulated by the polynomial of the normalized temperature, $\tau = T/T_{\mathrm{c}}^{\phi}$, and T_{c}^{ϕ} is the Curie temperature of solution for ferromagnetic ordering and β is the Bohr magneton number.

5. Optimized results and discussion

The optimization was carried out by using a PARROT program in Thermo-Calc software [50,51], which can handle various kinds of experimental data. The experimental data of the phase diagram and thermodynamic properties were used as input to the program. Each piece of selected information was given a certain weight by the importance of data, and changed by trial and error during the assessment, until most of the selected experimental information is reproduced within the expected uncertainty limits.

5.1. The Cu–Mn system

The calculated Cu–Mn phase diagram by the present assessment is shown in Fig. 2, where the reaction temperatures are labeled. A complete set of thermodynamic parameters describing the Gibbs free energy of each phase in this system is given in Table 1. The calculated results show that the eutectoid reactions (δMn) ↔ liquid + fcc and (βMn) ↔ (αMn) + fcc exist at 1373 and 977 K, respectively, which are in an excellent agreement with those reviewed by Gokcen [13]. A comparison between the calculated and experimental results is shown in Fig. 3. According to the calculation by the optimized parameters, the metastable miscibility gap of the fcc phase can be predicted in the Mn-rich portion, as shown in Fig. 3, where the highest critical temperatures is 976 K at 78 at.% Mn (75.4 wt.% Mn). The calculated critical temperature for the fcc phase is in good agreement with that thermodynamically analyzed by Kaufman and Bernstein [52], and is slightly higher than that reported by Vitek and War-

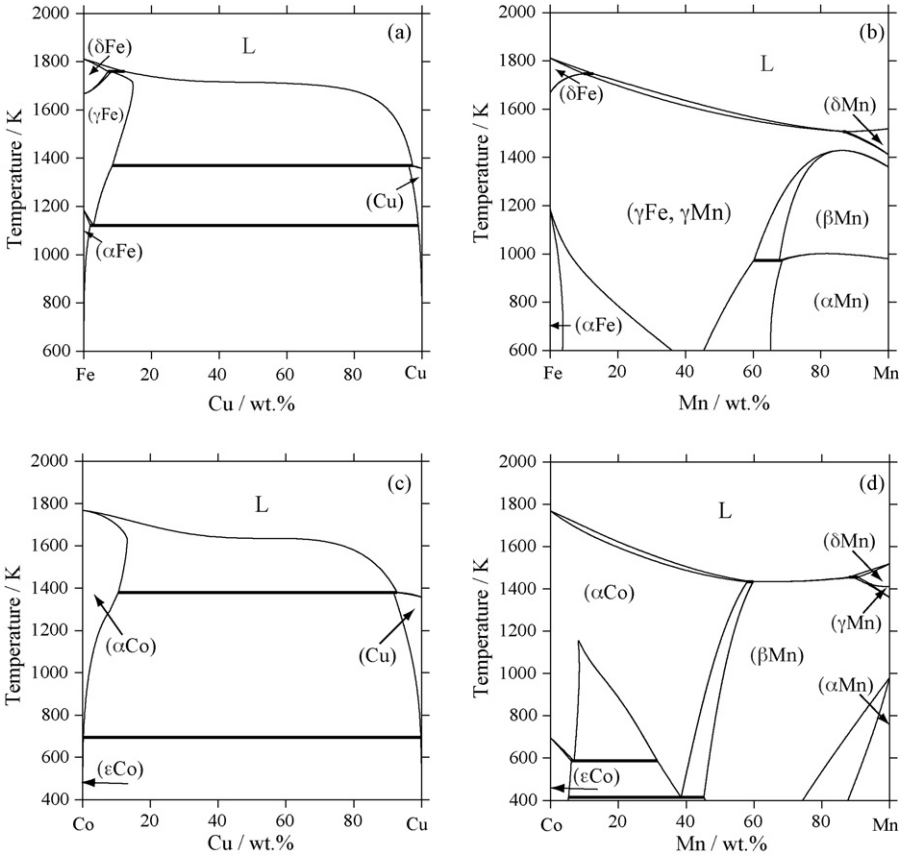

Fig. 8. Calculated binary phase diagrams of (a) Fe–Cu [53], (b) Fe–Mn [61], (c) Co–Cu [58], and (d) Co–Mn [65].

Table 2
Calculated reaction scheme in the Cu–Mn–X (Fe, Co) ternary system

Alloy system	Special point	Temperature (K)	Composition (wt.%)		
			Cu	Mn	X
Cu–Mn–Fe	C1	1714.0	9.59	10.65	79.76
	C2	1169.5	65.47	34.11	0.42
Cu–Mn–Co	C1	1409.1	3.26	70.96	25.78
	C2	1242.9	69.01	26.66	4.33

limont [5]. Fig. 4 shows the activities of Mn and Cu in the fcc phase compared with the experimental data. The features for the activities of Cu and Mn were well reproduced. The calculated activity values of Mn are in an agreement with the experimental data except the Mn-rich portion where the data show a rather scatter. The calculated activity of Cu is a basic agreement with the experimental data in the Cu- and Mn-rich parts, and it is found that there is a rapid change at about 60 at.% Mn (56.5 wt.% Mn). It is also seen that the calculated results are slightly lower than the observed ones in the middle composition range. Fig. 5 shows

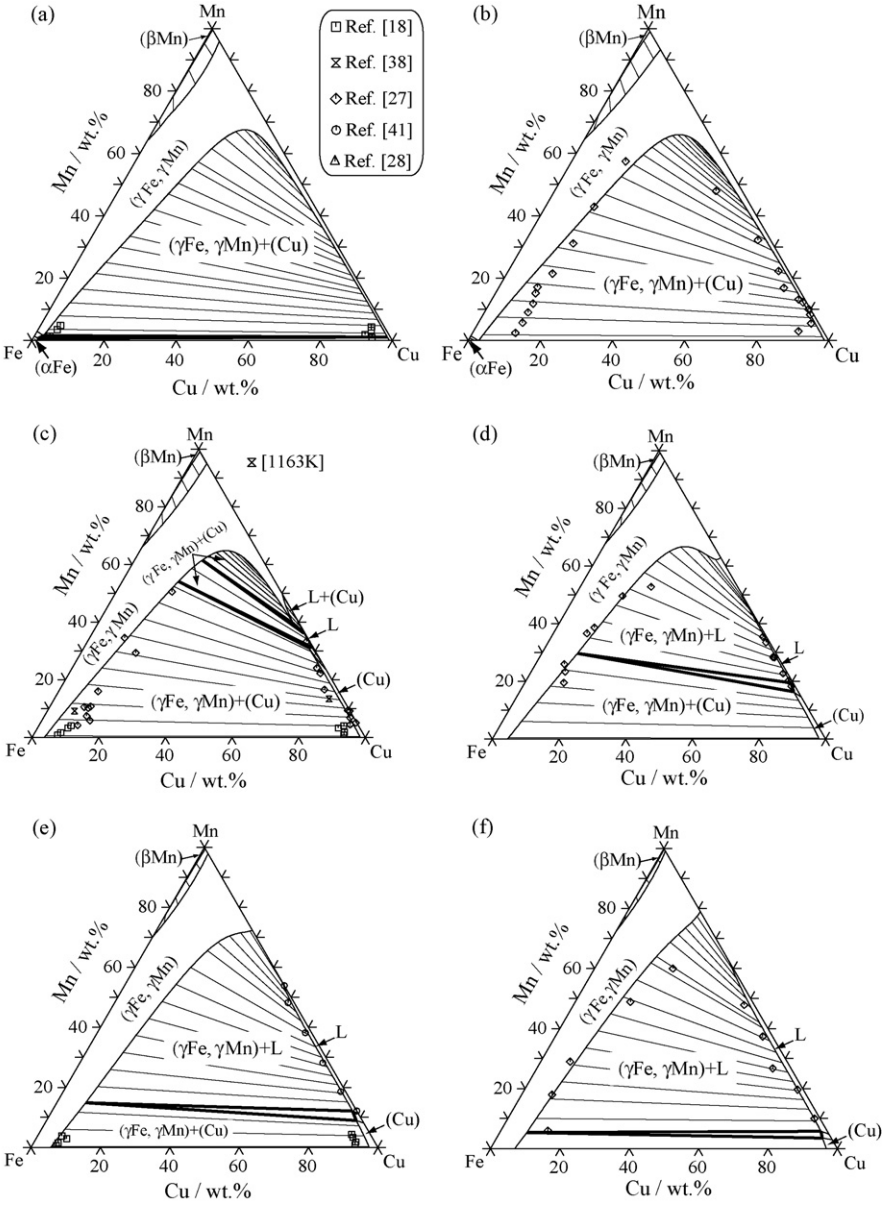

Fig. 9. Calculated isothermal section diagrams of the Cu–Mn–Fe system at (a) 1073 K, (b) 1123 K, (c) 1173 K, (d) 1223 K, (e) 1273 K, (f) 1323 K, (g) 1373 K, (h) 1473 K, and (i) 1573 K.

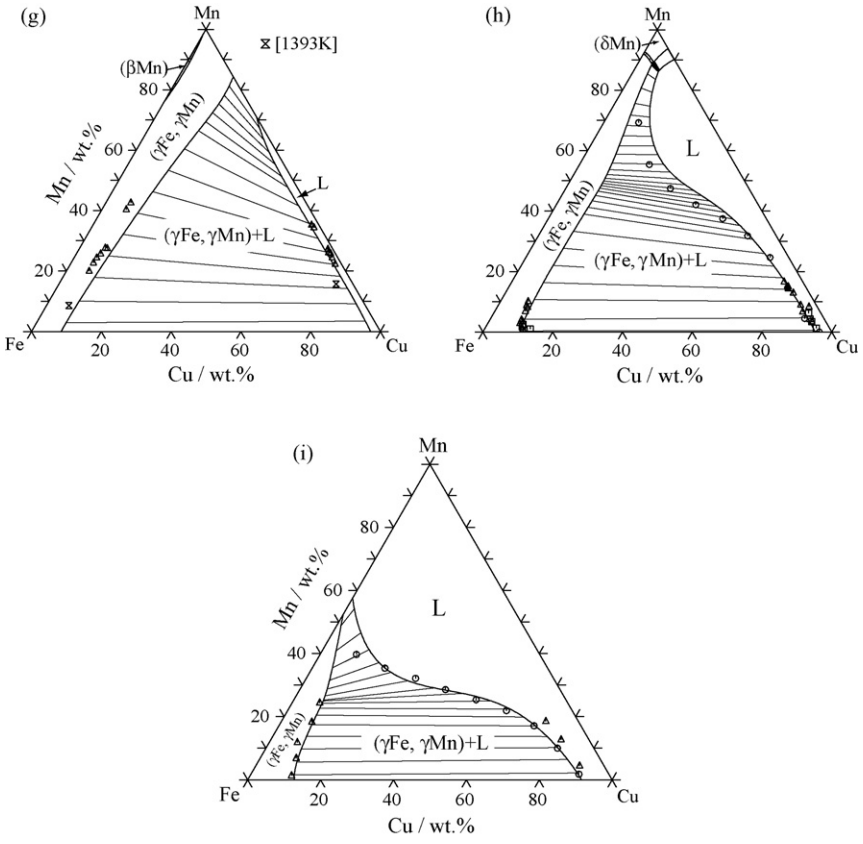

Fig. 9. (*Continued*).

the calculated iso-activity of Mn in the liquid and fcc phases compared with the selected experimental data. A comparison of the Gibbs free energy of mixing between calculated and experimental data is shown in Fig. 6. It is seen that a good agreement is obtained in the fcc phase, however, in liquid phase the calculated Gibbs free energy of mixing is slightly lower than the experimental values, but this is within the range of error. Fig. 7 shows a comparison of the heat capacity of the fcc phase between calculated and experimental values. It is seen that the data are scatter between 500 and 600 K, which was explained to be due to short-range ordering of the fcc phase [32]. In the present assessment, a better agreement between the calculated results and experimental data is obtained except for the data in the temperature range of 500–600 K because these data caused by short-range ordering cannot been reproduce by using the subregular solution model.

5.2. The Cu–Mn–X (X: Fe, Co) system

Several thermodynamic assessments of the Cu–Fe [53–57], Cu–Co [22,54,58–60], Mn–Fe [61–64], and Mn–Co [65] binary systems have been carried out by using CALPHAD method. The optimized parameters of the Cu–Fe [53], Cu–Co [58], Mn–Fe [61], and the Mn–Co [65] systems were used in the present work by considering the consistency of the thermodynamic database for the Cu-based alloys developed by our group [16,19,21]. The calculated these binary phase diagrams are shown in Fig. 8.

5.2.1. Cu–Mn–Fe system

The thermodynamic parameters of the Cu–Mn–Fe ternary system were evaluated on the basis of the experimental data of the phase equilibria because no thermodynamic properties are available, and are listed in Table 1. The calculated isothermal sections at 1073–1573 K are shown in Fig. 9. It is seen that the stable miscibility gap of the fcc phase exists in a large region in the Cu–Fe side at 1073–1323 K, and the calculated results are in good agreement with the experimental data. The calculated vertical sections at 10, 20 wt.% Mn, and 10, 20 wt.% Fe, and 10, 20 wt.% Cu also show a good agreement with the experimental data [39], as shown in Fig. 10. The calculated liquidus surface in the Cu–Mn–Fe ternary system is shown in Fig. 11 with superimposed data from Ref. [41]. Good agreement between the experimental data and calculated results was obtained. The lowest temperatures corresponding to two L + bcc (δFe) ↔ fcc1 (γFe, γMn), and L + fcc1 (γFe) ↔ fcc2 (Cu) reactions on the Mn-rich and Fe-rich corners are shown as points C1 and C2, respectively. The temperature and composition at points C1 and C2 are listed in Table 2, while the experimental data corresponding to the two points has not been reported.

5.2.2. Cu–Mn–Co system

The thermodynamic assessment of the Cu–Mn–Co system was performed based on the experimental data of the phase equilibria. The evaluated thermodynamic parameters of liquid, fcc, bcc and hcp phases are listed in Table 1. The calculated isother-

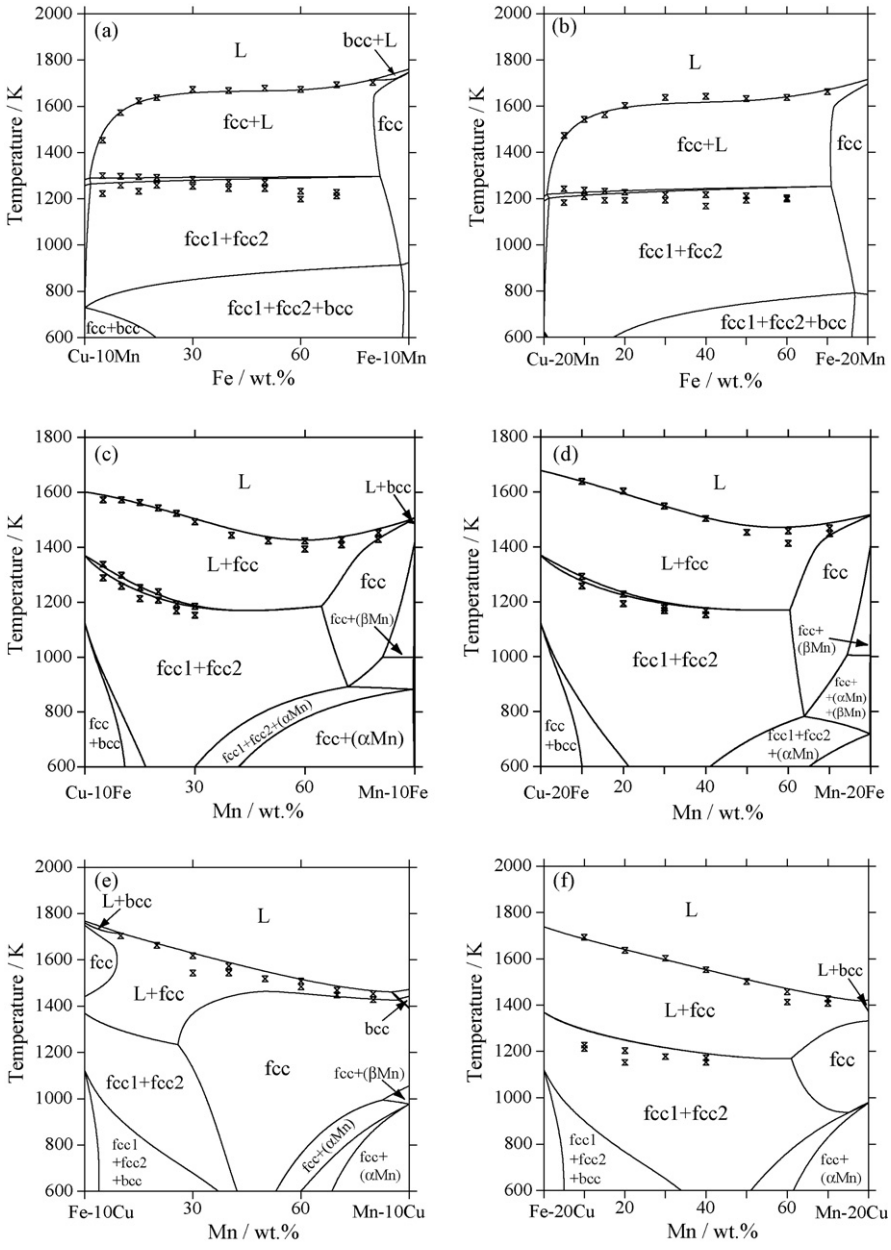

Fig. 10. Calculated (a) Mn = 10 wt.%, (b) Mn = 20 wt.%, (c) Fe = 10 wt.%, (d) Fe = 20 wt.%, (e) Cu = 10 wt.%, and (f) Cu = 20 wt.% vertical section diagrams including the experimental data [39] reviewed in Ref. [41] in the Cu–Mn–Fe system.

Table 3
Calculated invariant reaction in the Cu–Mn–Co ternary system

Reaction symbol	Reaction	Temperature (K)	Phase	Composition (wt.%)		
				Cu	Mn	Co
P	L + (βMn) + bcc → fcc	1450.1	L	0.62	87.18	12.20
			(βMn)	0.10	88.90	11.00
			bcc	0.32	90.16	9.52
			fcc	0.35	89.48	10.17

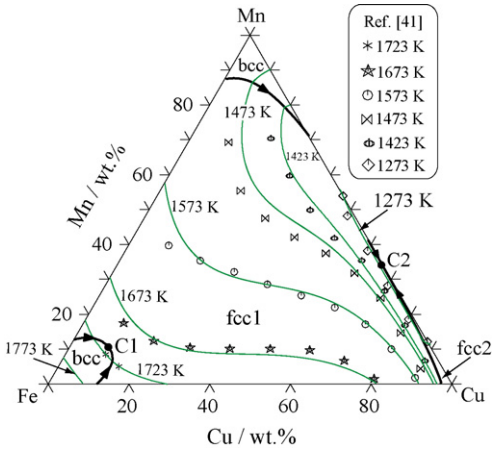

Fig. 11. Calculated liquidus of the Cu–Mn–Fe ternary system with superimposed data from [41].

mal section diagrams at 1050–1450 K are shown in Fig. 12. A good agreement between experimental data [31] and the calculated results was obtained. The phase equilibria in the Cu–Mn–Co system are similar to those in the Cu–Mn–Fe system, which indicates that the stable miscibility gap of the fcc phase also exists in a large region in the Cu–Co side. The calculated vertical sections at 10 and 20 wt.% Mn with the experimental data [45] are shown in Fig. 13, where the three-phase equilibrium of the fcc phase is predicted to exist in a temperature range of 600–1000 K. The calculated liquidus surface in the Cu–Mn–Co ternary system is shown in Fig. 14. No experimental data for the liquidus surface are available. On the basis of the calculated results, one eutectic invariant reaction, L + bcc (δMn) + (βMn) ↔ fcc1 (αCo) on the Co–Mn side in this system is predicted. The liquid composition of this reaction is shown in point P. The lowest temperatures corresponding to the L + fcc1

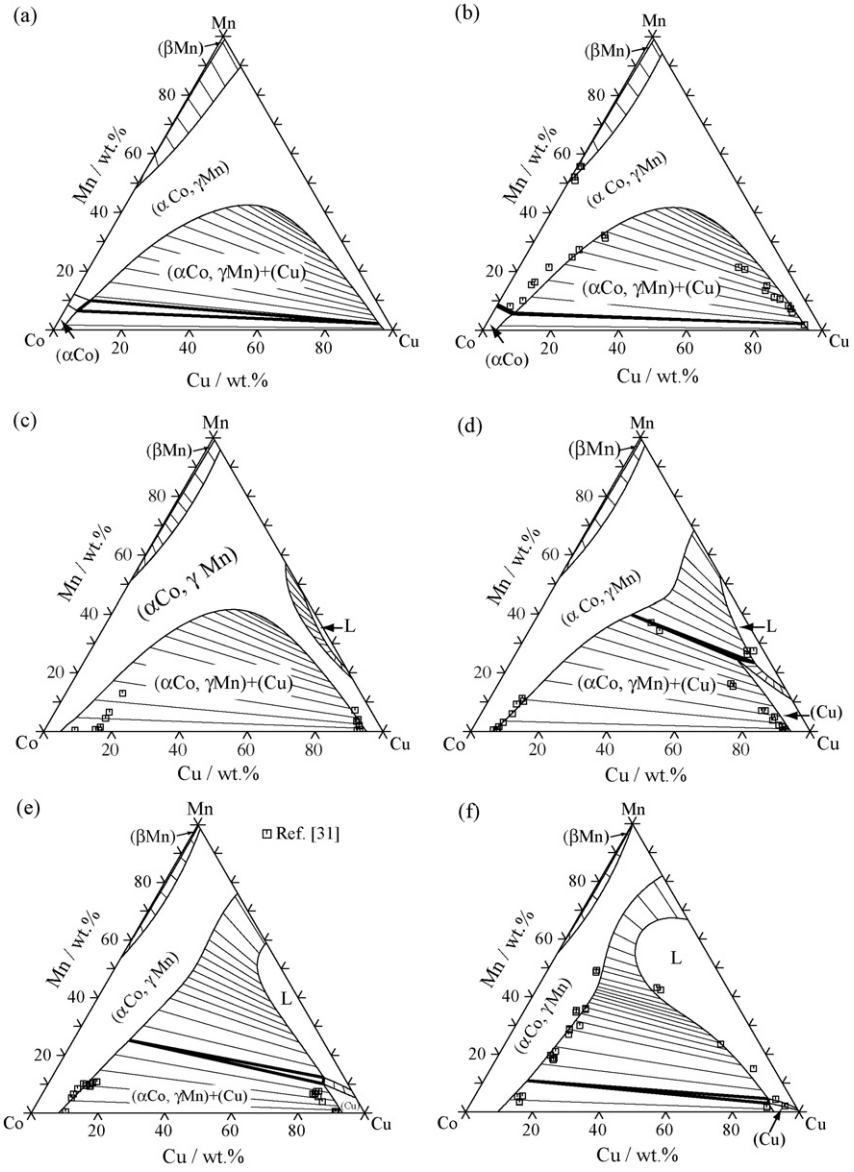

Fig. 12. Calculated isothermal section diagrams of the Cu–Mn–Co system with the experimental data of Ref. [31] at (a) 1050 K, (b) 1150 K, (c) 1200 K, (d) 1250 K, (e) 1300 K, (f) 1350 K, (g) 1400 K, and (h) 1450 K.

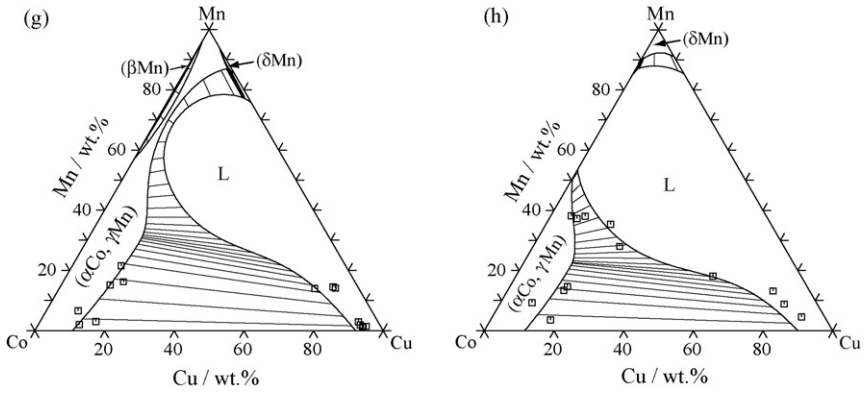

Fig. 12. (*Continued*).

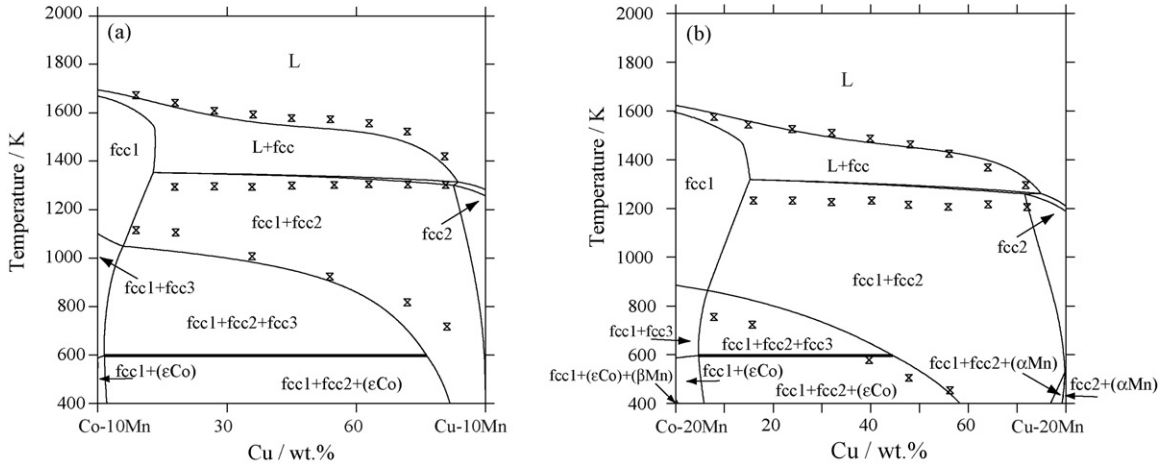

Fig. 13. Calculated (a) Mn = 10 wt.% and (b) Mn = 20 wt.% vertical section diagrams including the experimental data [45] reviewed in Ref. [46] in the Cu–Mn–Co system.

(αCo) ↔ (βMn) and L + fcc1 (αCo) ↔ fcc2 (Cu) reactions on the Co–Mn and Cu–Mn sides are shown as points C1 and C2, respectively. The temperatures and compositions for the points C1 and C2 are listed in Table 2, and eutectic invariant reaction is shown in Table 3.

5.3. Discussion on miscibility gap of the liquid phase

It is well known that there exists a metastable miscibility gap of the liquid phase at higher temperature in the Cu–Fe and Cu–Co binary systems [53,58,66,67], respectively. There is no miscibility gap of the liquid phase in the Cu–Mn, Fe–Mn and Co–Mn systems. On the basis of the present assessment, the calculated metastable miscibility gaps of the liquid phase is shown in Fig. 15, where the critical temperatures of the miscibility gaps in the Cu–Fe and Cu–Co quasi-binary systems decrease with increasing Mn content. As reported in our previous work, no stable miscibility gap of the liquid phase exists in the Cu–Mn–Fe system [18,30], and the same tendency of the

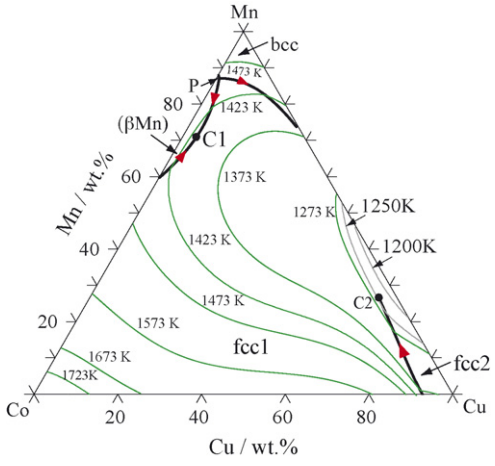

Fig. 14. Calculated liquidus of the Cu–Mn–Co ternary system.

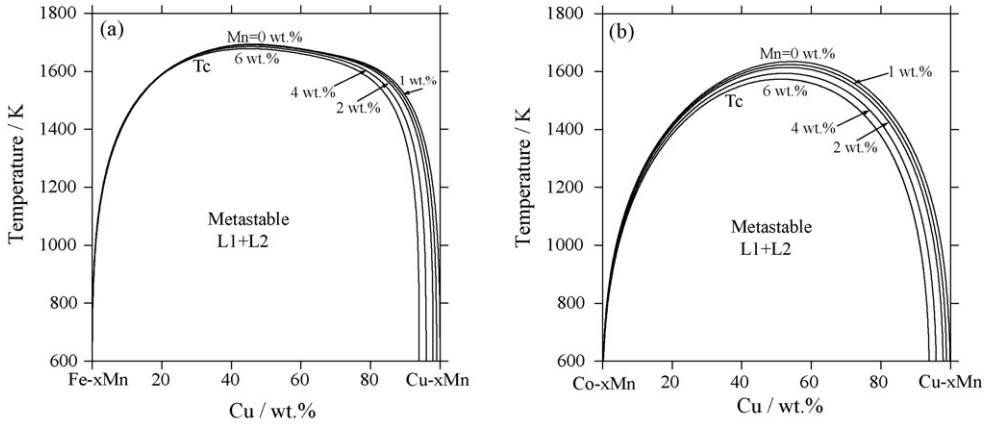

Fig. 15. Difference in the critical temperature of the miscibility gaps of the liquid phase with the additional Mn compositions in the (a) Fe–Cu quasi-binary system and (b) Co–Cu quasi-binary system.

liquid phase also exists in the Cu–Mn–Co ternary system, which is an effective guide for obtaining the separated microstructure of the Cu-rich and Fe-rich or Co-rich phases by using rapid solidification techniques [68–74].

6. Conclusions

(1) The Cu–Mn system was critically assessed by considering the phase equilibria and thermodynamic data, and most of experimental information can be satisfactorily reproduced on the basis of the optimized thermodynamic parameters.
(2) The thermodynamic assessments of the Cu–Mn–Fe and Cu–Mn–Co systems were made on the basis of the experimental data of the phase equilibria. A good agreement between the calculated results and experimental data is obtained.

Acknowledgements

This work was jointly supported by the National Natural Science Foundation of China, the Ministry of Science and Technology of the People's Republic of China, the Ministry of Education of the People's Republic of China, and Japan Science and Technology Agency (JST). The supports from Fujian International Cooperation Foundation and Fujian Natural Science Foundation are also acknowledged.

References

[1] R.J. Goodwin, Met. Sci. 2 (1968) 121.
[2] E.P. Butler, P.M. Kelly, Trans. Met. Soc. AIME 242 (1968) 2099.
[3] D.W. James, Mater. Sci. Eng. 4 (1969) 1.
[4] J.H. Smith, E.R. Vance, J. Appl. Phys. 40 (1969) 4853.
[5] J.M. Vitek, H. Warlimont, Met. Sci. (1976) 7.
[6] K. Kawahara, N. Sakuma, Y. Nishizaki, J. Jpn. Inst. Met. 57 (9) (1993) 1097.
[7] K. kawahara, N. Sakuma, Y. Nishizaki, J. Jpn. Inst. Met. 57 (9) (1993) 1089.
[8] G. Grube, E. Oestreicher, O. Winkler, Z. Elektrochem. 45 (1939) 776.
[9] R.S. Dean, J.R. Long, T.R. Graham, E.V. Potter, E.T. Hayes, Trans. ASM 34 (1945) 443.
[10] M. Kawasaki, K. Yamaji, O. Izumi, Sci. Rep. Res. Inst. Tohoku Univ. A 7 (1955) 443.
[11] A. Hellawell, W. Hume-Rothery, Philos. Trans. R. Soc. (London) A 249 (1957) 417.
[12] E. Wachtel, P. Terzieff, J. Bahlo, Monatshte für Chem. 117 (1986) 1349.
[13] N.A. Gokcen, in: P.R. Subramanian, D.J. Chakrabati, D.E. Laughlin (Eds.), Phase diagram of Binary Copper Alloys, ASM International, 1994, p. 253.
[14] L. Kaufman, H. Bernstein, in: A.M. Alper (Ed.), The Use of Phase Diagram in Ceramic Glass and Metal Technology, Academic Press, New York, 1970.
[15] C.P. Wang, X.J. Liu, I. Ohnuma, R. Kainuma, S.M. Hao, K. Ishida, Z. Metallkd. 89 (1998) 828.
[16] C.P. Wang, X.J. Liu, I. Ohnuma, R. Kainuma, K. Ishida, J. Phase Equilib. 21 (2000) 54.
[17] C.P. Wang, X.J. Liu, I. Ohnuma, R. Kainuma, K. Ishida, CALPHAD 24 (2000) 149.
[18] C.P. Wang, Doctor Thesis, Tohoku Univsersity, Japan, 2001.
[19] C.P. Wang, X.J. Liu, I. Ohnuma, R. Kainuma, K. Ishida, J. Phase Equilib. 23 (2002) 236.
[20] C.P. Wang, M. Jiang, X.J. Liu, I. Ohnuma, R. Kainuma, K. Ishida, Jpn. J. Copper Alloys 41 (2002) 176.
[21] C.P. Wang, X.J. Liu, M. Jiang, I. Ohnuma, R. Kainuma, K. Ishida, J. Phys. Chem. Solids 66 (2005) 256.
[22] L. Kaufman, CALPHAD 2 (1978) 117.
[23] K. Lewin, D. Sichen, S. Seetlaraman, Scand. J. Metall. 22 (1993) 310.
[24] J. Vřešt'ál, J. Štepánková, B. Rroz, Scand. J. Metall. 25 (1996) 224.
[25] J. Miettinen, CALPHAD 27 (1) (2003) 103.
[26] A.T. Dinsdale, CALPHAD 15 (1991) 317.
[27] M. Hasebe, T. Nishsawa, Application of Phase Diagrams in Metallurgy and Ceramics, NBS Special Publication 496 2, 1978, p. 910.
[28] H. Ohtani, H. Suta, K. Ishida, ISIJ Int. 37 (1997) 207.
[29] J. Miettinen, CALPHAD 27 (2003) 141.
[30] C.P. Wang, X.J. Liu, I. Ohnuma, R. Kainuma, K. Ishida, Metall. Mater. Trans. A 35A (2004) 1243.
[31] M. Hasebe, K. Oikawa, T. Nishizawa, J. Jpn. Inst. Met. 46 (6) (1982) 584.
[32] E. Scheil, W. Normann, Z. Metallkd. 51 (1960) 165.
[33] P.J. Spencer, J.N. Pratt, Trans. Faraday Soc. 64 (1968) 1470.
[34] R.W. Kremzer, M. Jool, Trans. Met. Soc. AIME 245 (1969) 91.
[35] K. Okajima, H. Sakao, Trans. Jpn. Inst. Met. 6 (1975) 87.
[36] J.P. Hajra, Scr. Metall. 13 (1979) 173.
[37] B.F. Peters, P.R. Wiles, Can. J. Chem. 41 (1963) 2591.
[38] W.J.M. Salter, J. Iron Steel Inst. 204 (1966) 478.
[39] N. Parravano, Int. Z. Metallogr. 4 (1913) 171.
[40] Y.A. Chang, in: Y.A. Chang (Ed.), Phase Diagrams and Thermodynamic Properties of Ternary Cooper–Metal System, Int. Copper Research Association, 1979, p. 588.
[41] G.V. Raynor, V.G. Rivlin, Phase Equilibria in Iron Ternary Alloys, vol. 4, The Institute of Metals, London, GB, 1988, p. 345.
[42] V. Raghavan, J. Phase Equilib. 15 (5) (1994) 542.

[43] P. Villars, A. Prince, H. Okamoto, Handbook of Ternary Alloy Phase Diagrams, vol. 7, ASM International, Materials Park, OH, 1995, p. 9336.
[44] K. Oikawa, Thesis of Master of Eng., Tohoku Univ., Japan, 1981.
[45] W. Köster, E. Wagner, Z. Metallkd. 30 (1938) 352.
[46] P. Villars, A. Prince, H. Okamoto, Handbook of Ternary Alloy Phase Diagrams, vol. 6, ASM International, Materials Park, OH, 1995, p. 8172.
[47] Y.A. Chang, in: Y.A. Chang (Ed.), Phase Diagrams and Thermodynamic Properties of Ternary Cooper–Metal System, Int. Copper Research Association, 1979, p. 422.
[48] O. Redlich, A.T. Kister, Ind. Eng. Chem. 40 (1948) 354.
[49] M. Hillert, M. Jarl, CALPHAD 2 (1978) 227.
[50] B. Jansson, Trita-Mac-0234, Division of Physical Metallurgy, Royal Institute of Technology, Stockholm, Sweden, 1984.
[51] B. Sundman, B. Jansson, J.-O. Andersson, CALPHAD 9 (1985) 153.
[52] L. Kaufman, H. Bernstein, Computer Calculation of Phase Diagram, Academic Press, New York, 1970.
[53] Q. Chen, Z.P. Jin, Metall. Mater. Trans. A 26A (1995) 417.
[54] M. Hasebe, T. Nishizawa, CALPHAD 4 (1980) 83.
[55] M.A. Turchanin, P.G. Agraval, I.V. Nikolaenko, J. Phase Equilibria 24 (2003) 307.
[56] A. Jansson, Report D73 Metallografi KTH (1986) also in SSOL database, ThermoCalc AB.
[57] Y.Y. Chuang, R. Schmid, Y.A. Chang, Metall. Mater. Trans. A 15A (1984) 1921.
[58] J. Kubišta, J. Vřešťál, J. Phase Equilib. 21 (2000) 125.
[59] C. Gente, M. Oehring, R. Bormann, Phys. Rev. B 48 (1993) 13244.
[60] M. Palumbo, S. Curiotto, L. Battezzati, CALPHAD 30 (2006) 171.
[61] W. Huang, CALPHAD 13 (1989) 243.
[62] W. Huang, CALPHAD 11 (1987) 183.
[63] B.-J. Lee, D.N. Lee, CALPHAD 13 (1989) 345.
[64] V.T. Witusiewicz, F. Sommer, E.J. Mittemeijer, J. Phase Equilib. 25 (4) (2004) 346.
[65] W. Huang, CALPHAD 13 (3) (1989) 231.
[66] H. Okamoto, Phase Diagram of Binary Iron Alloys, ASM International, Materials Park, OH, 1993, p. 131.
[67] H. Okamoto, P.R. Subramanian, L. Kacprzak, Desk Handbook Phase Diagram for Binary Alloys, ASM International, The Materials Information Society, 2000, p. 1181.
[68] Y. Nakagawa, Acta Metall. 6 (1958) 704.
[69] G. Wilde, R. Willnecker, R.N. Singh, F. Sommer, Z. Metallk. 88 (10) (1997) 804.
[70] M.B. Robinson, D. Li, T.J. Rathz, G. Williams, J. Mater. Sci. 34 (1999) 3747.
[71] S. Amara, A. Belhadj, R. Kesri, S.H. Thibault, Z. Metallk. 90 (2) (1999) 116.
[72] D.I. Kim, R. Abbaschian, J. Phase Equilib. 21 (1) (2000) 25.
[73] X.Y. Lu, C.D. Cao, B. Wei, Mater. Sci. Eng. A 313 (2001) 198.
[74] C.D. Cao, G.P. Görler, D.M. Herlach, B. Wei, Mater. Sci. Eng. A 325 (2002) 503.